THE JOURNAL OF PHYSICAL CHEMISTRY Letters

pubs.acs.org/JPCL Letter

Femtosecond Soft-X-ray Absorption Spectroscopy of Liquids with a Water-Window High-Harmonic Source

Adam D. Smith,[¶] Tadas Balčiūnas,[¶] Yi-Ping Chang, Cédric Schmidt, Kristina Zinchenko, Fernanda B. Nunes, Emanuele Rossi, Vít Svoboda, Zhong Yin,* Jean-Pierre Wolf, and Hans Jakob Wörner*

Cite This: *J. Phys. Chem. Lett.* 2020, 11, 1981−1988 Read Online

ACCESS | Metrics & More | Article Recommendations | Supporting Information

ABSTRACT: Femtosecond X-ray absorption spectroscopy (XAS) is a powerful method to investigate the dynamical behavior of a system after photoabsorption in real time. So far, the application of this technique has remained limited to large-scale facilities, such as femtosliced synchrotrons and free-electron lasers (FEL). In this work, we demonstrate femtosecond time-resolved soft-X-ray absorption spectroscopy of liquid samples by combining a sub-micrometer-thin flat liquid jet with a high-harmonic tabletop source covering the entire water-window range (284−538 eV). Our work represents the first extension of tabletop XAS to the oxygen edge of a chemical sample in the liquid phase. In the time domain, our measurements resolve the gradual appearance of absorption features below the carbon K-edge of ethanol and methanol during strong-field ionization and trace the valence-shell ionization dynamics of the liquid alcohols with a temporal resolution of ∼30 fs. This technique opens unique opportunities to study molecular dynamics of chemical systems in the liquid phase with elemental, orbital, and site sensitivity.

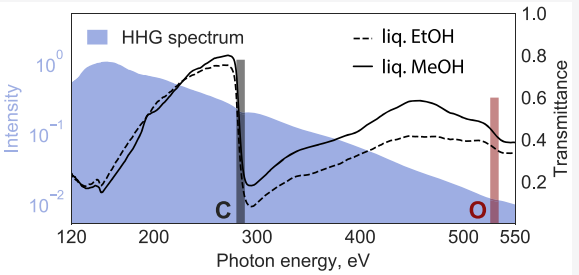

Time-resolved X-ray absorption spectroscopy (TRXAS) has evolved into a powerful tool to investigate the structural and electronic dynamics of matter with elemental, site, and orbital specificity.[1−5] Earlier TRXAS experiments were performed at synchrotron facilites with a temporal resolution limited by the synchrotron pulse duration to 50−100 ps.[6] However, the fundamental time scale of nuclear motion lies in the femtosecond range. The rapid technical development of synchrotrons and FELs has led to a substantial improvement of the time resolution over the last years. The slicing technique at synchrotron facilities achieved femtosecond resolution at the cost of a low photon flux.[7] The development of FELs has led to X-ray pulses with femtosecond time resolution at much higher photon fluxes, which enabled remarkable scientific progress in femtosecond protein nanocrystallography, chemical dynamics, as well as catalysis, material, and energy research.[2,8−12,12−22] However, X-ray absorption measurements at FEL are experimentally challenging due to large shot-to-shot fluctuations. Recent efforts concentrated on new X-ray optics developments, where the sample and reference signal can be obtained simultaneously.[23,24] Nevertheless, the first step of photoinduced dynamics is an electronic excitation, which occurs on a time scale faster than nuclear motion, calling for even higher temporal resolution.

In parallel to the developments at accelerator facilities, tabletop sources also considerably increased their performance in terms of photon flux, photon energy, and time resolution. Plasma-based sources can provide photon energies reaching the keV regime with sub-ps time resolution.[25,26] Light sources based on high-harmonic generation (HHG) can also reach up to keV in energy, but due to the inherently coherent emission process, they also reach attosecond time resolution.[27−30] Furthermore, the time and energy resolution are not interdependent through the uncertainty principle and can, therefore, be optimized separately. Thus, the ultrabroad spectral coverage of HHG is ideally suited for ultrafast X-ray absorption measurements. Additionally, the common optical origin of the pump and probe pulses enable a near-perfect temporal synchronization to be achieved.

Pioneering transient-absorption experiments via HHG were performed using near-infrared (NIR)-laser-based sources with a cutoff limited to the extreme ultraviolet (XUV) photon-energy range.[31] Ultrafast dynamics of transition-metal compounds as well as magnetization and spin-transfer dynamics have been studied using XUV sources.[32−36] In this energy range, electrons from the valence orbitals and a few shallow core levels can be reached, and thus, element-specific

Received: December 3, 2019
Accepted: February 19, 2020
Published: February 19, 2020

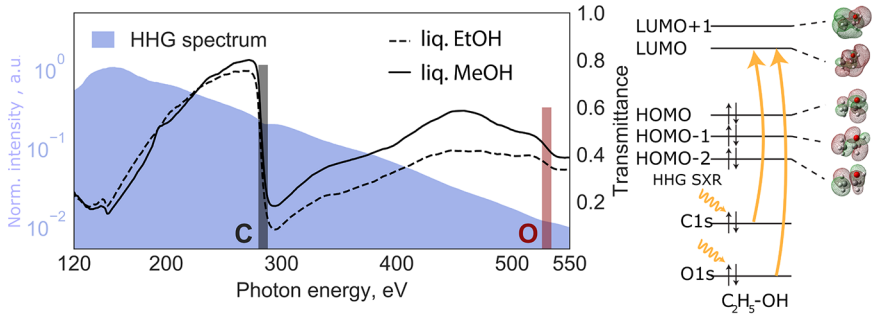

Figure 1. Left: Static SXR absorption spectra. The shaded area is the high-harmonic spectrum displayed on a logarithmic intensity scale. The dashed and solid lines represent the transmittance spectra of liquid ethanol and methanol, respectively, through a sub-micrometer-thin flat liquid jet. These overview spectra have been recorded with the MCP detector. Right: Schematic representation of the molecular orbitals of the ethanol molecule using the 6-31G** basis set and the observed X-ray transitions.

information is difficult to obtain. Deep-lying core electrons provide element sensitivity, and furthermore, their binding energies are site- and orbital-specific. The energy required to excite these electrons in organic molecules is in the soft-X-ray (SXR) range, since the molecules contain carbon, nitrogen, or oxygen. Very recent progress in optical parametric amplified laser sources[37,38] enabled the generation of SXR spectra covering the water-window regime[39−43] and first applications to time-resolved measurements in gases.[44,45]

In addition to broadband ultrashort light sources, SXR absorption spectroscopy requires targets that are thinner than one absorption length to avoid spectral artifacts and signal distortions.[46,47] For condensed samples in the SXR domain, the absorption lengths typically amount to hundreds of nm. Implementing liquid samples that are sufficiently thin proved to be experimentally challenging. The additional vacuum requirements further added to the complexity of the experimental setup. The development of homogeneous flat microjets[48,49] has very recently enabled the first observation of high-order harmonic generation in liquids,[50] the measurement of static SXR absorption spectra of aqueous solutions recorded with an HHG source,[51] and the dynamical investigation of metal complexes at a synchrotron facility with ∼50 ps temporal resolution.[52]

Here, we report the first realization of femtosecond SXR absorption spectroscopy in the liquid phase utilizing an HHG source in the water-window region[39] and a sub-micrometer flat jet.[50] We study the femtosecond dynamics following the strong-field ionization of alcohols. We demonstrate a temporal resolution of ∼30 fs and the formation of pre-edge absorption features arising from the creation of an outer-valence hole in liquid ethanol and methanol. We assign the observed transitions from the 1s orbital of carbon to the highest-lying occupied molecular orbital (HOMO, or valence band) and the lowest-lying molecular orbital (LUMO, or conduction band). This development establishes the feasibility of femtosecond time-resolved SXR experiments in liquids, which have the potential of driving major advances in our understanding of electronic and structural dynamics in solvated systems.

The laser source consisting of a high-power femtosecond laser system, an optical parametric amplifier, and a filamentation-based pulse compressor as well as the HHG source and the SXR beamline are described in the Experimental and Theoretical Methods, which includes an overview of the experimental setup. Briefly, the output of a cryogenically cooled titanium−sapphire (Ti:Sa) laser system is used to pump an optical parametric amplifier delivering ∼1.6 mJ pulses centered at ∼1800 nm. These pulses are compressed to a duration of ∼13 fs, i.e., two to three optical cycles using a two-stage filamentation pulse compressor. The beam is then focused into a gas target filled with helium at a pressure of ∼3.5 bar, resulting in HHG spectra extending up to ∼550 eV. The high-harmonic radiation subsequently interacts with a flat liquid microjet at normal incidence. The transmitted radiation is spectrally analyzed in a flat-field SXR spectrometer. The pump pulses with a central wavelength of 400 nm and a pulse duration of ∼30 fs are created by frequency doubling a small fraction of the 800 nm output of the Ti:Sa laser system. The frequency doubling was performed to minimize the spectral perturbations in the strong-field interactions with the liquid sample. The pump beam intersects the SXR probe beam under a small angle (0.5°) inside the flat microjet.

We report overview spectra with very wide spectral coverage at relatively low spectral resolution as well as high-resolution spectra with narrower spectral coverage. The low-resolution spectra were recorded with a spectrometer equipped with a microchannel-plate (MCP) detector, whereas the high-resolution spectra were taken with an X-ray charge-coupled-device (CCD) camera. The raw HHG spectrum measured in the absence of the flatjet is shown in Figure 1 as the blue-shaded area. It spans the energy range from 120 to 550 eV, covering the entire water window. The maximum flux is observed at 150 eV, followed by a monotonic decrease until the cutoff, which is located at approximately 550 eV. The spectrum notably covers the entire water window from the carbon K-edge to the oxygen K-edge, as well as lower energies, enabling the recording of time-resolved X-ray absorption spectra at many edges simultaneously, such as the K-edges of B, C, N, and O as well as the L-edges of P, S, Cl, Ar, among others. This extremely broad spectral coverage is the key distinguishing feature of our tabletop laser-based source in comparison with a FEL.

The transmittance spectra through the liquid methanol and ethanol samples are shown in Figure 1 as the solid and dashed lines, respectively. Both spectra show the characteristic increase in absorption around the C K-edge located at ∼288 eV, represented by the black-shaded rectangle in the figure. The O K-edge is also clearly observed at ∼538 eV (red-shaded rectangle). To the best of our knowledge, this represents the first observation of absorption at the O K-edge of a liquid sample using an HHG source. The absorption at the O K-edge is significantly weaker because of the much lower atomic absorption cross section. An additional contributing effect may come from the photon flux which is one order of magnitude

https://dx.doi.org/10.1021/acs.jpclett.9b03559
J. Phys. Chem. Lett. 2020, 11, 1981−1988

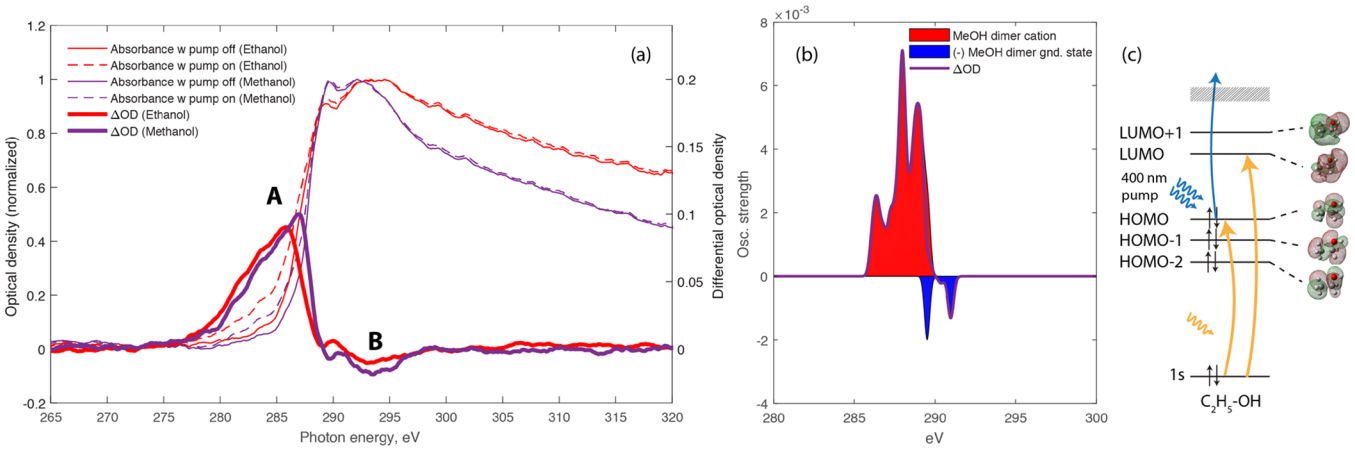

Figure 2. Transient SXR absorption spectra at the carbon K-edge. (a) Measured absorption spectra of neutral ethanol and methanol before (thin solid lines) and after (dashed lines) strong-field ionization. The pumped spectra were averaged over delays ranging from t = 50−250 fs. The difference spectra ΔOD are shown as thick solid lines. These data have been recorded with the CCD camera. (b) Calculated X-ray absorption spectrum of the methanol dimer cation (red area) and neutral methanol dimer in its ground state (blue area) spectra. The spectra of the cation have been obtained by integration over the simulated time interval. The difference between the two spectra, corresponding to the ΔOD, is shown as a solid purple line. (c) Schematic representation of the molecular orbitals of the ethanol molecule and the observed X-ray transitions.

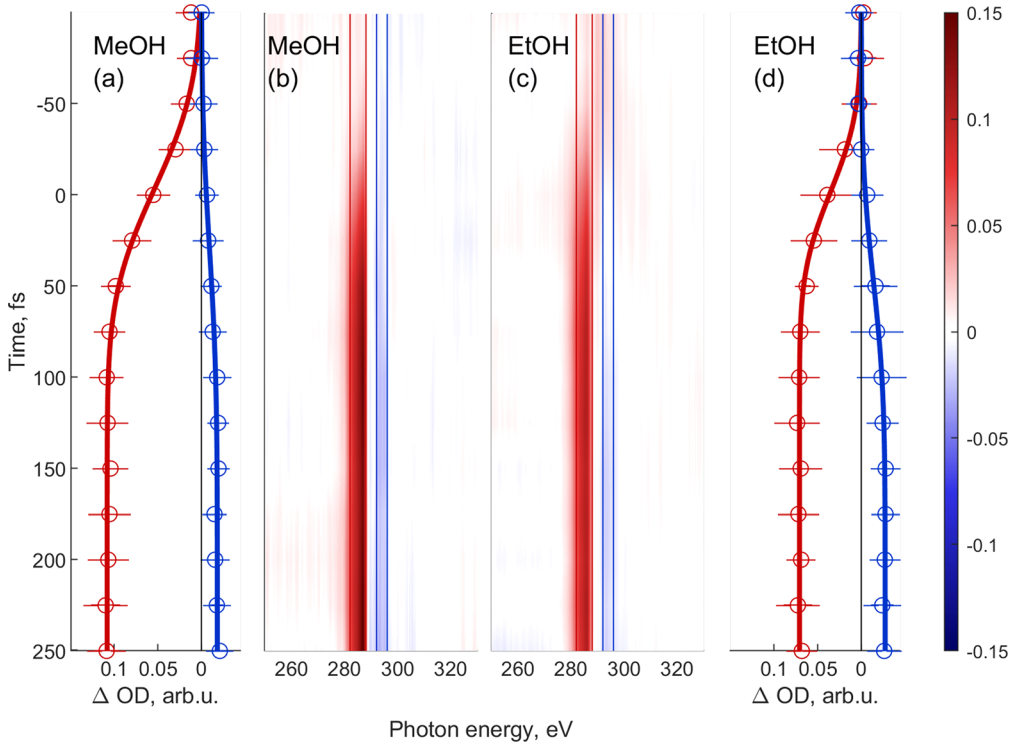

Figure 3. Time evolution of the transient absorption spectrum (ΔOD) of methanol (a,b) and ethanol (c,d). Panels (a) and (b) indicate the lineouts of the highlighted spectral regions in the corresponding ΔOD maps (b) and (c). The lineouts were fitted using sigmoidal functions, such that the exact onset of the feature can be determined. Energy ranges are 284−288 eV and 283−287 eV for the positive absorption bands (marked red) and 292−296 eV and 292−296 eV (marked blue) in the case of methanol and ethanol, respectively. These data have been recorded with the CCD camera.

weaker compared to the C K-edge, making the O K-edge signals more susceptible to residual background offset. The difference in transmittance at the C K-edge between ethanol and methanol is due to the unequal number of carbon atoms within each molecule and a possible difference in sample thickness.

For the time-resolved measurements, we concentrate on the carbon K-edge because of the higher spectral resolution. Figure 2 shows the absorption spectra of liquid methanol and ethanol as thin violet and red solid lines, respectively. The spectra have been normalized to their maximum within the displayed energy range and show the characteristic increase of absorption between 285 and 290 eV, corresponding to transitions from the carbon 1s to the lowest unoccupied orbitals (or conduction bands).[53] They additionally show absorption features above the absorption edge, which originate from transitions into the photo−ionization continuum. These structures are similar between methanol and ethanol in displaying a relatively sharp

https://dx.doi.org/10.1021/acs.jpclett.9b03559
J. Phys. Chem. Lett. 2020, 11, 1981−1988

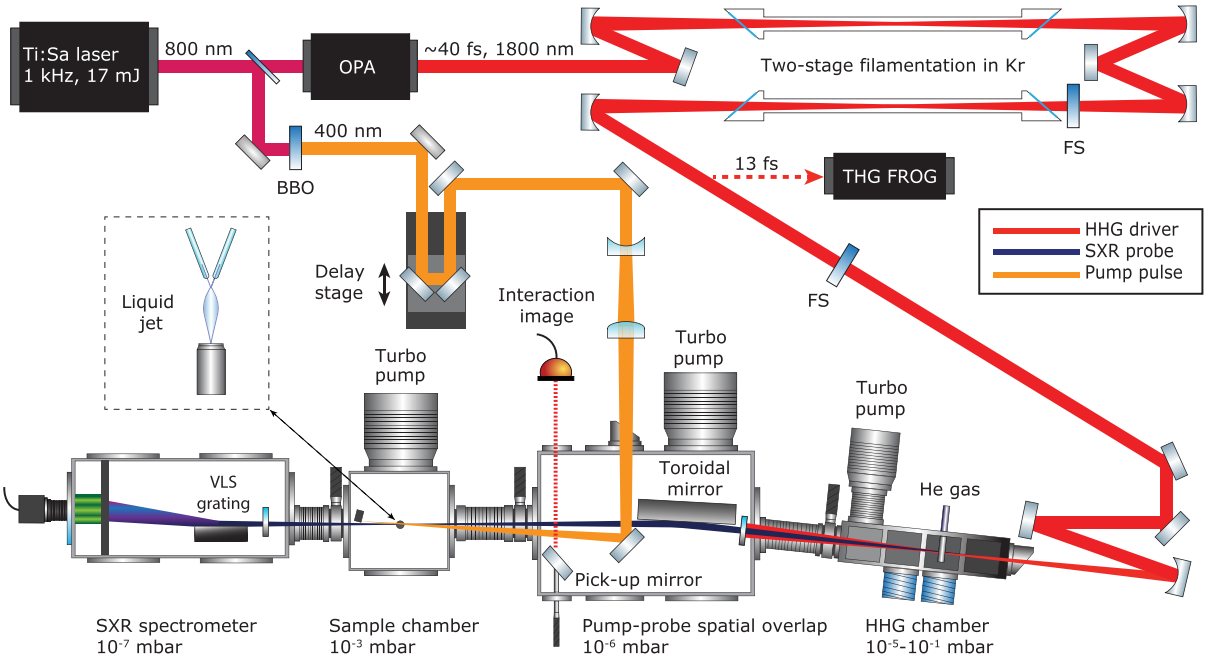

Figure 4. Experimental setup, showing both the light sources and the SXR beamline. The pump and probe pulses are overlapped on the liquid flat jet. The small crossing angle of 0.5° ensures negligible temporal smearing of <3 fs. The inset illustrates the geometry of the flat-jet sample and the liquid-nitrogen cold trap that captures the majority of the liquid. The SXR probe is generated in a differentially pumped high-harmonic gas cell and refocused using a toroidal mirror. Finally, the spectrometer consists of a flat-field grating and an X-ray CCD camera.

peak with a width of ~1.5 eV, followed by a broader spectral feature, although the amplitudes of these features are different between the two alcohols. By comparison with prior work on X-ray absorption of liquid methanol[53,54] and methanol clusters,[55] the narrow peak can be assigned to two main transitions from the carbon 1s orbital to final-state orbitals with dominant σ^*(O−H) and σ^*(C−H) characters. The broader peak can similarly be assigned to a dominant transition to a final−state orbital of σ^*(C−O) and σ^*(C−H) character. The first pre-edge of the static ethanol absorption is shifted toward lower energy compared to methanol. This could be due to the presence of the second carbon, which has a lower 1s binding energy according to gas-phase experiments.[53,56] We note that comparison of our data with previous results on liquid methanol may suggest saturation effects caused by a larger sample thickness compared to ethanol.

Figure 2 further shows the corresponding absorption spectra following the action of the strong-field-ionization pump pulse as dashed lines using the same color coding. The changes in absorption are relatively minor, which indicates a small ionization fraction resulting from the relatively weak pump pulse of ~1 × 10^{14} W/cm^2. The dominant visible changes are an increased absorption below the respective absorption edges. The spectral changes induced by the pump pulse are better visible in the difference spectra, in which they are shown as thick full lines. The absorption spectra in the presence of the pump pulse, as well as the difference spectra, have been averaged over pump−probe delays ranging from ~50 to ~250 fs. The difference spectra have additionally been multiplied by a factor of 5 to highlight the spectral structures of the small changes in absorption. The dominant features in the difference spectra are the increased absorption below the respective absorption edges displaying a monotonic increase from 277 eV to 285−287 eV labeled as A, followed by a sharp decrease and negative contributions (B) that mirror the sharp and broad spectral features observed in the spectra of the unpumped liquids.

We now turn to the observation of femtosecond time-resolved changes in the absorption spectra. The time-resolved measurements shown in Figure 3 span the time delay range from −125 to 250 fs in 25 fs steps, where positive delays correspond to the pump pulse arriving before the probe pulse. These data have been recorded with the CCD camera to achieve a higher spectral resolution. At every time step, two spectra are recorded with 10 images and 4 s of exposure time each for the pump-on (strong-field ionization) and pump-off cases. In order to calculate the ΔOD spectra, defined as the difference between pump-on and pump-off absorbances ΔOD = $A_{pump} - A_{ref}$, we first averaged all images for a specific time step.[44] In Figure 3, we present time-resolved measurements in ethanol and methanol. The data in panels B and C are false-color representations of ΔOD as a function of time delay and photon energy. In both of them, a strong broad feature around 285 eV can be observed, which corresponds to the C K-edge for each molecule. The features appear in the spectra around time zero and remain approximately constant throughout the measured delay range. For the interpretation of our data, we performed electronic structure calculations of *ab initio* molecular dynamics (AIMD) sampled methanol dimers based on the density functional theory (see Experimental and Theoretical Methods for details). The calculated spectra are shown in Figure 2(b). The theoretical results reproduce well the monomer spectra of methanol, see Figure S4, and the additional band below the pre-edge, which originates from the transition from the 1s of carbon to the HOMO vacancy. These calculations further predict a proton transfer to occur from the ionized methanol molecule to its hydrogen-bond acceptor on an ultrafast time scale. The AIMD results show how the internuclear separation of one OH bond of a methanol molecule in a dimer configuration elongates in the first tens of

https://dx.doi.org/10.1021/acs.jpclett.9b03559
J. Phys. Chem. Lett. 2020, 11, 1981−1988

femtoseconds, while the distance of the same hydrogen to the oxygen atom of the neighboring methanol molecule shrinks (see the Supporting Information Figures S5 and S6). This finding is in agreement with a previous work, which also showed evidence for proton-transfer dynamics after valence ionization of a methanol dimer in the first tens of femtoseconds.[57] However, a dimer is only a rudimentary model for the liquid phase, and therefore, these results cannot be expected to quantitatively agree with our experimental data.

Panels A and D represent the energy integration over the ΔOD signal between the positive and negative bands and fits of sigmoidal functions to the data (see Figure 3 caption for the corresponding photon-energy ranges). The rise times of the positive and negative ΔOD bands are associated with the dynamics of strong-field ionization of liquid ethanol and methanol. The positive absorption feature can be associated with transitions from the C 1s core level to the HOMO orbital (or band), which was dominantly ionized by the strong laser field. The rise times of the positive ΔOD bands, defined as an amplitude change from 10 to 90%, amount to 69 ± 10 fs and 52 ± 9 fs in methanol and ethanol, respectively. These rise times are notably slower than the duration of the pump pulse, which indicates that the observed dynamics are not exclusively electronic in character but also involve nuclear motion. Our own calculations as well as previous theoretical work on the ionization-induced dynamics of methanol clusters indeed predict an ultrafast proton transfer to take place following ionization,[57] offering a possible explanation for the observed noninstantaneous response.

We have successfully performed the first time-resolved SXR absorption measurements in the liquid phase using a high-harmonic source. This source is sufficiently broad to simultaneously cover the energy range from 100 to 550 eV, covering both the carbon and the oxygen K-edges. The present results show the formation of an outer-valence hole during strong-field ionization of liquid alcohols. The appearance of the corresponding pre-edge absorption features at the carbon K-edge was observed to be notably slower than the experimental time resolution, which is attributed to the participation of nuclear dynamics triggered by ionization. These results demonstrate the potential of such experiments, especially their unique combination of broad spectral coverage with high temporal resolution, which will enable unprecedented insights to be obtained on liquid-phase dynamics using the element and site sensitivity of X-ray spectroscopy.

EXPERIMENTAL AND THEORETICAL METHODS

An overview of the experimental setup is shown in Figure 4. The primary light source consists of a Ti:sapphire regenerative amplifier providing 4 mJ pulses that are subsequently amplified in a cryogenically cooled two-pass amplifier (Coherent Inc.). The two-stage Ti:sapphire-based laser system provides 17 mJ, 40 fs pulses at a 1 kHz repetition rate. Its output is used to pump a BBO-based type-II parametric amplifier seeded with a white-light supercontinuum originating from the same pump pulse. The parametric amplifier delivers ∼1.6 mJ, 40 fs idler pulses centered at λ = 1.8 μm wavelength that are passively carrier-envelope-phase (CEP) stable. This mid-IR output is then compressed down to sub-three-cycle pulses in a dual-filamentation setup. Details regarding the optimization of the HHG source are given in ref 39. The water-window-spanning SXR spectrum is generated by focusing the compressed pulses using a f = 250 mm spherical mirror into a static high-pressure helium gas target (3.5 bar) via high-order harmonic generation. The SXR beam is then refocused using a nickel-coated grazing-incidence toroidal mirror from ARW Optical Corp. onto the liquid flat jet, resulting in a focal spot size of 62 μm on target. The pump pulse is obtained by splitting a 10% fraction of the 800 nm laser beam and then frequency doubling it in a BBO crystal. The pump pulses were characterized using self-diffraction frequency-resolved optical gating (FROG), which provided a measured pulse length of ∼30 fs. The pump beam of the experiment was passed over a delay stage and focused onto the target using a spherical-mirror-based telescopic focusing system with an effective focal length of 1.5 m resulting in a peak intensity of $\sim 1 \times 10^{14}$ W/cm^2.

The transmitted SXR probe pulse spectrum was recorded with a soft-X-ray spectrometer based on a blazed variable-line-spacing grating from Hitachi with a 2400 line/mm density in the center.[58] The overview spectra shown in Figure 1 were recorded with a 40 mm active diameter MCP phosphor and optical detector, whereas the data shown in Figures 2 and 3 were recorded with a backilluminated enhanced coated Newton X-ray CCD camera from Andor with a nominal pixel size of 13.5 × 13.5 μm. The effective pixel size of the CCD is smaller than the MCP's and therefore led to a higher energy resolution, see also ref 59.

The flat microjet is created by colliding two cylindrical microjets created from 18 μm inner-diameter quartz nozzles using a high-pressure liquid chromatography pump, resulting in a flat jet with a sheet thickness of <600 nm, based on an extrapolation of thickness measurements performed with white-light interferometry. The flat-jet setup has been previously described in ref 50 and has been further optimized to reach sub-micrometer thickness. The thickness depends on various parameters, such as the orifice size of the nozzle, flow rate, type of liquid, and position of the measurement with respect to the flat microjet. The flow rate for the creation of a stable flat microjet in turn depends on the nozzle orifice size and the viscosity of the sample. For the presented experiments, the flow rate was 1.2 mL/min. Absolute pure ethanol and methanol liquids with at least 99.8% purity from Merck were used. A liquid-nitrogen cold trap and differential pumping maintained a pressure of $<1 \times 10^{-3}$ mbar in the liquid-jet chamber and $<5 \times 10^{-7}$ mbar in the spectrometer chamber with a running flat jet.

To minimize the photon-flux fluctuations, each ΔOD spectrum was referenced by recording two spectra with the pump beam unblocked/blocked. For every time delay step, 10 such pairs of spectra were acquired. The information is then used to calculate the error bars in Figure 3, panels (a) and (d).

The time evolution of the absorption spectrum was modeled by calculating it at various successive molecular configurations utilizing an AIMD calculation. At the beginning of the time evolution, the molecular system was chosen to be in its electronic ground state. The corresponding coordinates were adopted from ref 60. Following ionization, AIMD calculations were used to simulate the time evolution of the singly charged system. A 500 fs long trajectory with a 0.2 fs time step was calculated using the GAUSSIAN 09 package[61] using the extended Lagrangian approach.[62] The 6-31G* basis set and the B3LYP exchange-correlation functional (XC) were employed. The time evolution of the spectrum was accounted for by sampling the geometry of the system in the AIMD trajectory every 5 fs. The C K-edge spectrum corresponding to each geometry was calculated. Each spectrum was calculated by

https://dx.doi.org/10.1021/acs.jpclett.9b03559
J. Phys. Chem. Lett. 2020, 11, 1981−1988

means of unrestricted DFT calculations using the Amsterdam Density Functional package (ADF version 2016.107). The Slater type basis sets utilized were ET-QZ3P-3DIFFUSE for the C atom and TZP for both the O and the H atoms. The XC utilized was X3LYP because of its more accurate description of the intermolecular interactions.[63−65] The spectral calculations were performed with the DFT transition state (DFT-TS) scheme.[66,67] In particular, the transition potential (TP) scheme was adopted, introducing a single half electron (charge-wise) in the carbon 1s orbital.[66,67] In the context of this scheme, the excitation energies were calculated as the difference between the Kohn−Sham (KS) eigenvalues relative to the final (φ_f^{TS}) and the initial (φ_i^{TS}) KS orbitals of the excitation. The probability of absorption was evaluated from

$$f = \frac{2}{3} n_i \Delta E_{i\to f} |\langle \varphi_i^{TS} | \hat{\mu} | \varphi_f^{TS} \rangle|^2 \quad (1)$$

where n_i is the occupation number of the initial state, $\Delta E_{i\to f}$ is the energy of the transition, and $\hat{\mu}$ is the dipole operator. The line spectrum obtained was convoluted with a Gaussian profile of 0.4 eV FWHM, corresponding to the spectrometer resolution.

■ ASSOCIATED CONTENT

Supporting Information

The Supporting Information is available free of charge at https://pubs.acs.org/doi/10.1021/acs.jpclett.9b03559.

SXR probe and optical pump beams characterization; SXR spectrometer description and resolution analysis; theoretical simulations (PDF)

■ AUTHOR INFORMATION

Corresponding Authors

Zhong Yin − *Laboratory of Physical Chemistry, ETH Zürich, 8093 Zürich, Switzerland*; Email: yinz@ethz.ch

Hans Jakob Wörner − *Laboratory of Physical Chemistry, ETH Zürich, 8093 Zürich, Switzerland*; orcid.org/0000-0002-8877-0872; Email: hwoerner@ethz.ch

Authors

Adam D. Smith − *Laboratory of Physical Chemistry, ETH Zürich, 8093 Zürich, Switzerland*

Tadas Balčiūnas − *GAP-Biophotonics, Université de Genève, 1205 Geneva, Switzerland*

Yi-Ping Chang − *GAP-Biophotonics, Université de Genève, 1205 Geneva, Switzerland*

Cédric Schmidt − *GAP-Biophotonics, Université de Genève, 1205 Geneva, Switzerland*

Kristina Zinchenko − *Laboratory of Physical Chemistry, ETH Zürich, 8093 Zürich, Switzerland*

Fernanda B. Nunes − *Laboratory of Physical Chemistry, ETH Zürich, 8093 Zürich, Switzerland*

Emanuele Rossi − *Laboratory of Physical Chemistry, ETH Zürich, 8093 Zürich, Switzerland*

Vít Svoboda − *Laboratory of Physical Chemistry, ETH Zürich, 8093 Zürich, Switzerland*

Jean-Pierre Wolf − *GAP-Biophotonics, Université de Genève, 1205 Geneva, Switzerland*

Complete contact information is available at: https://pubs.acs.org/10.1021/acs.jpclett.9b03559

Author Contributions

¶A.D.S. and T.B. contributed equally

Funding

This work was supported by ETH Zurich, the Swiss National Science Foundation (SNSF) through the NCCR−MUST and project (20021_172946) and an ERC Consolidator Grant (772797-ATTOLIQ). T.B. acknowledges financial support from a Marie-Curie fellowship grant agreement No 798176. Z.Y. acknowledges financial support from an ETH Career Seed Grant No SEED-12 19-1.

Notes

The authors declare no competing financial interest.

■ ACKNOWLEDGMENTS

It is our pleasure to thank Andreas Schneider, Mario Seiler, Andres Laso, and Markus Kerellaj for their contributions to the construction of the experiment and Michel Moret for his precious technical assistance. Z.Y. thanks N. Kosugi for sharing unpublished results.

■ REFERENCES

(1) De Groot, F. High-resolution X-ray emission and X-ray absorption spectroscopy. *Chem. Rev.* **2001**, *101*, 1779−1808.

(2) Chen, L. X.; Jäger, W. J.; Jennings, G.; Gosztola, D. J.; Munkholm, A.; Hessler, J. P. Capturing a photoexcited molecular structure through time-domain X-ray absorption fine structure. *Science* **2001**, *292*, 262−264.

(3) Penfold, T. J.; Milne, C. J.; Chergui, M. Recent advances in ultrafast x-ray absorption spectroscopy of solutions. *Adv. Chem. Phys.* **2013**, *153*, 1−41.

(4) Yano, J.; Yachandra, V. K. X-ray absorption spectroscopy. *Photosynth. Res.* **2009**, *102*, 241.

(5) Bressler, C.; Chergui, M. Ultrafast X-ray absorption spectroscopy. *Chem. Rev.* **2004**, *104*, 1781−1812.

(6) Thiel, D. J.; Livins, P.; Stern, E. A.; Lewis, A. Microsecond-resolved XAFS of the triplet excited state of $Pt_2(P_2O_5H_2)^{4-}{}_4$. *Nature* **1993**, *362*, 40.

(7) Schoenlein, R.; Chattopadhyay, S.; Chong, H.; Glover, T.; Heimann, P.; Shank, C.; Zholents, A.; Zolotorev, M. Generation of femtosecond pulses of synchrotron radiation. *Science* **2000**, *287*, 2237−2240.

(8) Bressler, C.; Milne, C.; Pham, V.-T.; Elnahhas, A.; van der Veen, R. M.; Gawelda, W.; Johnson, S.; Beaud, P.; Grolimund, D.; Kaiser, M.; et al. Femtosecond XANES study of the light-induced spin crossover dynamics in an iron(II) complex. *Science (Washington, DC, U. S.)* **2009**, *323*, 489−92.

(9) Chapman, H. N.; Fromme, P.; Barty, A.; White, T. A.; Kirian, R. A.; Aquila, A.; Hunter, M. S.; Schulz, J.; DePonte, D. P.; Weierstall, U.; et al. Femtosecond X-ray protein nanocrystallography. *Nature* **2011**, *470*, 73.

(10) Erk, B.; Boll, R.; Trippel, S.; Anielski, D.; Foucar, L.; Rudek, B.; Epp, S. W.; Coffee, R.; Carron, S.; Schorb, S.; et al. Imaging charge transfer in iodomethane upon x-ray photoabsorption. *Science* **2014**, *345*, 288−291.

(11) Huse, N.; Wen, H.; Nordlund, D.; Szilagyi, E.; Daranciang, D.; Miller, T. A.; Nilsson, A.; Schoenlein, R. W.; Lindenberg, A. M. Probing the hydrogen-bond network of water via time-resolved soft x-ray spectroscopy. *Phys. Chem. Chem. Phys.* **2009**, *11*, 3951−3957.

(12) Kern, J.; Alonso-Mori, R.; Tran, R.; Hattne, J.; Gildea, R. J.; Echols, N.; Glöckner, C.; Hellmich, J.; Laksmono, H.; Sierra, R. G.; et al. Simultaneous femtosecond X-ray spectroscopy and diffraction of photosystem II at room temperature. *Science* **2013**, *340*, 491−495.

(13) Bostedt, C.; Boutet, S.; Fritz, D. M.; Huang, Z.; Lee, H. J.; Lemke, H. T.; Robert, A.; Schlotter, W. F.; Turner, J. J.; Williams, G. J. Linac coherent light source: The first five years. *Rev. Mod. Phys.* **2016**, *88*, 015007.

(14) Suga, M.; Akita, F.; Sugahara, M.; Kubo, M.; Nakajima, Y.; Nakane, T.; Yamashita, K.; Umena, Y.; Nakabayashi, M.; Yamane, T.; et al. Light-induced structural changes and the site of O=O bond formation in PSII caught by XFEL. *Nature* **2017**, *543*, 131.
(15) Schneider, R.; Mehringer, T.; Mercurio, G.; Wenthaus, L.; Classen, A.; Brenner, G.; Gorobtsov, O.; Benz, A.; Bhatti, D.; Bocklage, L.; et al. Quantum imaging with incoherently scattered light from a free-electron laser. *Nat. Phys.* **2018**, *14*, 126.
(16) Dong, W. J.; Lee, J.-L. Tailoring Oxidation State of Solution-Processed MoO_{3-x} Layer Using Laser-Irradiation and Its Application in Organic Solar Cells. *Adv. Mater. Interfaces* **2019**, *6*, 1901195.
(17) Cavalleri, A.; Tóth, C.; Siders, C. W.; Squier, J.; Ráksi, F.; Forget, P.; Kieffer, J. Femtosecond structural dynamics in VO 2 during an ultrafast solid-solid phase transition. *Phys. Rev. Lett.* **2001**, *87*, 237401.
(18) Radu, I.; Vahaplar, K.; Stamm, C.; Kachel, T.; Pontius, N.; Dürr, H.; Ostler, T.; Barker, J.; Evans, R.; Chantrell, R.; et al. Transient ferromagnetic-like state mediating ultrafast reversal of antiferromagnetically coupled spins. *Nature* **2011**, *472*, 205.
(19) Shelby, M. L.; Lestrange, P. J.; Jackson, N. E.; Haldrup, K.; Mara, M. W.; Stickrath, A. B.; Zhu, D.; Lemke, H. T.; Chollet, M.; Hoffman, B. M.; et al. Ultrafast excited state relaxation of a metalloporphyrin revealed by femtosecond x-ray absorption spectroscopy. *J. Am. Chem. Soc.* **2016**, *138*, 8752−8764.
(20) Haumann, M.; Liebisch, P.; Müller, C.; Barra, M.; Grabolle, M.; Dau, H. Photosynthetic O2 formation tracked by time-resolved X-ray experiments. *Science* **2005**, *310*, 1019−1021.
(21) Smolentsev, G.; Guda, A.; Zhang, X.; Haldrup, K.; Andreiadis, E. S.; Chavarot-Kerlidou, M.; Canton, S. E.; Nachtegaal, M.; Artero, V.; Sundstrom, V. Pump-flow-probe X-ray absorption spectroscopy as a tool for studying intermediate states of photocatalytic systems. *J. Phys. Chem. C* **2013**, *117*, 17367−17375.
(22) Obara, Y.; Ito, H.; Ito, T.; Kurahashi, N.; Thürmer, S.; Tanaka, H.; Katayama, T.; Togashi, T.; Owada, S.; Yamamoto, Y.-i.; et al. Femtosecond time-resolved X-ray absorption spectroscopy of anatase TiO2 nanoparticles using XFEL. *Struct. Dyn.* **2017**, *4*, 044033.
(23) Katayama, T.; Inubushi, Y.; Obara, Y.; Sato, T.; Togashi, T.; Tono, K.; Hatsui, T.; Kameshima, T.; Bhattacharya, A.; Ogi, Y.; et al. Femtosecond x-ray absorption spectroscopy with hard x-ray free electron laser. *Appl. Phys. Lett.* **2013**, *103*, 131105.
(24) Brenner, G.; Dziarzhytski, S.; Miedema, P. S.; Rösner, B.; David, C.; Beye, M. Normalized single-shot X-ray absorption spectroscopy at a free-electron laser. *Opt. Lett.* **2019**, *44*, 2157−2160.
(25) Ráksi, F.; Wilson, K. R.; Jiang, Z.; Ikhlef, A.; Côté, C. Y.; Kieffer, J. Ultrafast x-ray absorption probing of a chemical reaction. *J. Chem. Phys.* **1996**, *104*, 6066−6069.
(26) Iqbal, M.; Urrehman, Z.; Im, H.; Son, J.; Seo, O.; Stiel, H.; Nickles, P.; Noh, D.; Janulewicz, K. Performance improvement of a Kα source by a high-resolution thin-layer-graphite spectrometer and a polycapillary lens. *Appl. Phys. B: Lasers Opt.* **2014**, *116*, 305−311.
(27) Popmintchev, T.; Chen, M.-C.; Popmintchev, D.; Arpin, P.; Brown, S.; Alisauskas, S.; Andriukaitis, G.; Balciunas, T.; Mucke, O. D.; Pugzlys, A.; et al. Bright Coherent Ultrahigh Harmonics in the keV X-ray Regime from Mid-Infrared Femtosecond Lasers. *Science* **2012**, *336*, 1287−1291.
(28) Gaumnitz, T.; Jain, A.; Pertot, Y.; Huppert, M.; Jordan, I.; Ardana-Lamas, F.; Wörner, H. J. Streaking of 43-attosecond soft-X-ray pulses generated by a passively CEP-stable mid-infrared driver. *Opt. Express* **2017**, *25*, 27506−27518.
(29) Li, J.; Ren, X.; Yin, Y.; Zhao, K.; Chew, A.; Cheng, Y.; Cunningham, E.; Wang, Y.; Hu, S.; Wu, Y.; et al. 53-attosecond X-ray pulses reach the carbon K-edge. *Nat. Commun.* **2017**, *8*, 186.
(30) Cousin, S. L.; Di Palo, N.; Buades, B.; Teichmann, S. M.; Reduzzi, M.; Devetta, M.; Kheifets, A.; Sansone, G.; Biegert, J. Attosecond Streaking in the Water Window: A New Regime of Attosecond Pulse Characterization. *Phys. Rev. X* **2017**, *7*, 41030.
(31) Goulielmakis, E.; Loh, Z.-H.; Wirth, A.; Santra, R.; Rohringer, N.; Yakovlev, V. S.; Zherebtsov, S.; Pfeifer, T.; Azzeer, A. M.; Kling, M. F.; et al. Real-time observation of valence electron motion. *Nature* **2010**, *466*, 739−743.
(32) Hofherr, M.; Häuser, S.; Dewhurst, J.; Tengdin, P.; Sakshath, S.; Nembach, H.; Weber, S.; Shaw, J.; Silva, T.; Kapteyn, H.; et al. Ultrafast optically induced spin transfer in ferromagnetic alloys. *Science Advances* **2020**, *6*, No. eaay8717.
(33) Kfir, O.; Zayko, S.; Nolte, C.; Sivis, M.; Möller, M.; Hebler, B.; Arekapudi, S. S. P. K.; Steil, D.; Schäfer, S.; Albrecht, M.; et al. Nanoscale magnetic imaging using circularly polarized high-harmonic radiation. *Science advances* **2017**, *3*, No. eaao4641.
(34) Siegrist, F.; Gessner, J. A.; Ossiander, M.; Denker, C.; Chang, Y.-P.; Schröder, M. C.; Guggenmos, A.; Cui, Y.; Walowski, J.; Martens, U.; et al. Light-wave dynamic control of magnetism. *Nature* **2019**, *571*, 240−244.
(35) Vura-Weis, J.; Jiang, C.-M.; Liu, C.; Gao, H.; Lucas, J. M.; de Groot, F. M. F.; Yang, P.; Alivisatos, A. P.; Leone, S. R. Femtosecond M2,3-Edge Spectroscopy of Transition-Metal Oxides: Photoinduced Oxidation State Change in α-Fe2O3. *J. Phys. Chem. Lett.* **2013**, *4*, 3667−3671.
(36) Zhang, K.; Lin, M.-F.; Ryland, E. S.; Verkamp, M. A.; Benke, K.; de Groot, F. M. F.; Girolami, G. S.; Vura-Weis, J. Shrinking the Synchrotron: Tabletop Extreme Ultraviolet Absorption of Transition-Metal Complexes. *J. Phys. Chem. Lett.* **2016**, *7*, 3383−3387.
(37) Fuji, T.; Ishii, N.; Teisset, C. Y.; Gu, X.; Metzger, T.; Baltuska, A.; Forget, N.; Kaplan, D.; Galvanauskas, A.; Krausz, F. Parametric amplification of few-cycle carrier-envelope phase-stable pulses at 2.1 μm. *Opt. Lett.* **2006**, *31*, 1103−1105.
(38) Silva, F.; Teichmann, S. M.; Cousin, S. L.; Hemmer, M.; Biegert, J. Spatiotemporal isolation of attosecond soft X-ray pulses in the water window. *Nat. Commun.* **2015**, *6*, 6611.
(39) Schmidt, C.; Pertot, Y.; Balciunas, T.; Zinchenko, K.; Matthews, M.; Wörner, H. J.; Wolf, J.-P. High-order harmonic source spanning up to the oxygen K-edge based on filamentation pulse compression. *Opt. Express* **2018**, *26*, 11834.
(40) Teichmann, S. M.; Silva, F.; Cousin, S. L.; Hemmer, M.; Biegert, J. 0.5-keV Soft X-ray attosecond continua. *Nat. Commun.* **2016**, *7*, 11493.
(41) Johnson, A. S.; Austin, D. R.; Wood, D. A.; Brahms, C.; Gregory, A.; Holzner, K. B.; Jarosch, S.; Larsen, E. W.; Parker, S.; Strüber, C. S.; et al. High-flux soft x-ray harmonic generation from ionization-shaped few-cycle laser pulses. *Science Advances* **2018**, *4*, eaar3761.
(42) Popmintchev, D.; Galloway, B. R.; Chen, M. C.; Dollar, F.; Mancuso, C. A.; Hankla, A.; Miaja-Avila, L.; O'Neil, G.; Shaw, J. M.; Fan, G.; et al. Near- and Extended-Edge X-Ray-Absorption Fine-Structure Spectroscopy Using Ultrafast Coherent High-Order Harmonic Supercontinua. *Phys. Rev. Lett.* **2018**, *120*, 093002.
(43) Buades, B.; Picón, A.; León, I.; Di Palo, N.; Cousin, S. L.; Cocchi, C.; Pellegrin, E.; Martin, J. H.; Mañas-Valero, S.; Coronado, E. et al. Attosecond-resolved petahertz carrier motion in semi-metallic TiS2. *arXiv:1808.06493* 2018, *cond-mat.mtrl-sci*.
(44) Pertot, Y.; Schmidt, C.; Matthews, M.; Chauvet, A.; Huppert, M.; Svoboda, V.; von Conta, A.; Tehlar, A.; Baykusheva, D.; Wolf, J.-P. P.; et al. Time-resolved x-ray absorption spectroscopy with a water window high-harmonic source. *Science* **2017**, *355*, 264−267.
(45) Attar, A. R.; Bhattacherjee, A.; Pemmaraju, C.; Schnorr, K.; Closser, K. D.; Prendergast, D.; Leone, S. R. Femtosecond x-ray spectroscopy of an electrocyclic ring-opening reaction. *Science* **2017**, *356*, 54−59.
(46) Eisebitt, S.; Böske, T.; Rubensson, J.-E.; Eberhardt, W. Determination of absorption coefficients for concentrated samples by fluorescence detection. *Phys. Rev. B: Condens. Matter Mater. Phys.* **1993**, *47*, 14103.
(47) Nagasaka, M.; Yuzawa, H.; Horigome, T.; Kosugi, N. Reliable absorbance measurement of liquid samples in soft X-ray absorption spectroscopy in transmission mode. *J. Electron Spectrosc. Relat. Phenom.* **2018**, *224*, 93−99.

https://dx.doi.org/10.1021/acs.jpclett.9b03559
J. Phys. Chem. Lett. 2020, 11, 1981−1988

(48) Ekimova, M.; Quevedo, W.; Faubel, M.; Wernet, P.; Nibbering, E. T. J. A liquid flatjet system for solution phase soft-x-ray spectroscopy. *Struct. Dyn.* **2015**, *2*, 054301.
(49) Koralek, J. D.; Kim, J. B.; Bruža, P.; Curry, C. B.; Chen, Z.; Bechtel, H. A.; Cordones, A. A.; Sperling, P.; Toleikis, S.; Kern, J. F.; et al. Generation and characterization of ultrathin free-flowing liquid sheets. *Nat. Commun.* **2018**, *9*, 1353.
(50) Luu, T. T.; Yin, Z.; Jain, A.; Gaumnitz, T.; Pertot, Y.; Ma, J.; Wörner, H. J. Extreme-ultraviolet high-harmonic generation in liquids. *Nat. Commun.* **2018**, *9*, 3723.
(51) Kleine, C.; Ekimova, M.; Goldsztejn, G.; Raabe, S.; Strüber, C.; Ludwig, J.; Yarlagadda, S.; Eisebitt, S.; Vrakking, M. J. J.; Elsaesser, T.; et al. Soft X-ray Absorption Spectroscopy of Aqueous Solutions Using a Table-Top Femtosecond Soft X-ray Source. *J. Phys. Chem. Lett.* **2019**, *10*, 52−58.
(52) Fondell, M.; Eckert, S.; Jay, R. M.; Weniger, C.; Quevedo, W.; Niskanen, J.; Kennedy, B.; Sorgenfrei, F.; Schick, D.; Giangrisostomi, E.; et al. Time-resolved soft X-ray absorption spectroscopy in transmission mode on liquids at MHz repetition rates. *Struct. Dyn.* **2017**, *4*, 054902.
(53) Nagasaka, M.; Mochizuki, K.; Leloup, V.; Kosugi, N. Local structures of methanol−water binary solutions studied by soft X-ray absorption spectroscopy. *J. Phys. Chem. B* **2014**, *118*, 4388−4396.
(54) Wilson, K. R.; Cavalleri, M.; Rude, B. S.; Schaller, R. D.; Catalano, T.; Nilsson, A.; Saykally, R.; Pettersson, L. X-ray absorption spectroscopy of liquid methanol microjets: Bulk electronic structure and hydrogen bonding network. *J. Phys. Chem. B* **2005**, *109*, 10194−10203.
(55) Tamenori, Y.; Okada, K.; Takahashi, O.; Arakawa, S.; Tabayashi, K.; Hiraya, A.; Gejo, T.; Honma, K. Hydrogen bonding in methanol clusters probed by inner-shell photoabsorption spectroscopy in the carbon and oxygen K-edge regions. *J. Chem. Phys.* **2008**, *128*, 124321.
(56) Sham, T.; Yang, B.; Kirz, J.; Tse, J. K-edge near-edge x-ray-absorption fine structure of oxygen-and carbon-containing molecules in the gas phase. *Phys. Rev. A: At., Mol., Opt. Phys.* **1989**, *40*, 652.
(57) Tachikawa, H. Dynamics of ionization processes of methanol dimer: a direct ab initio dynamics study. *Chem. Phys.* **1999**, *244*, 263−272.
(58) Harada, T.; Takahashi, K.; Sakuma, H.; Osyczka, A. Optimum design of a grazing-incidence flat-field spectrograph with a spherical varied-line-space grating. *Appl. Opt.* **1999**, *38*, 2743−2748.
(59) Yin, Z.; Peters, H. B.; Hahn, U.; Agåker, M.; Hage, A.; Reininger, R.; Siewert, F.; Nordgren, J.; Viefhaus, J.; Techert, S. A new compact soft x-ray spectrometer for resonant inelastic x-ray scattering studies at PETRA III. *Rev. Sci. Instrum.* **2015**, *86*, 093109.
(60) Umer, M.; Leonhard, K. Ab initio calculations of thermochemical properties of methanol clusters. *J. Phys. Chem. A* **2013**, *117*, 1569−1582.
(61) Frisch, M. J. et al. *Gaussian 09*. Gaussian, Inc.: Wallingford CT, 2009.
(62) Car, R.; Parrinello, M. Unified approach for molecular dynamics and density-functional theory. *Phys. Rev. Lett.* **1985**, *55*, 2471.
(63) Santra, B.; Michaelides, A.; Fuchs, M.; Tkatchenko, A.; Filippi, C.; Scheffler, M. On the accuracy of density-functional theory exchange-correlation functionals for H bonds in small water clusters. II. The water hexamer and van der Waals interactions. *J. Chem. Phys.* **2008**, *129*, 194111.
(64) te Velde, G.; Bickelhaupt, F. M.; Baerends, E. J.; Fonseca Guerra, C.; van Gisbergen, S. J. A.; Snijders, J. G.; Ziegler, T. Chemistry with ADF. *J. Comput. Chem.* **2001**, *22*, 931.
(65) Fonseca Guerra, C.; Snijders, J. G.; te Velde, G.; Baerends, E. J. Towards an order-N DFT method. *Theor. Chem. Acc.* **1998**, *99*, 391.
(66) Slater, J. C. Statistical Exchange-Correlation in the Self-Consistent Field. *Adv. Quantum Chem.* **1972**, *6*, 1−92.
(67) De Francesco, R.; Stener, M.; Fronzoni, G. Theoretical study of near-edge X-ray absorption fine structure spectra of metal phthalocyanines at C and N K-edges. *J. Phys. Chem. A* **2012**, *116*, 2885−2894.

https://dx.doi.org/10.1021/acs.jpclett.9b03559
J. Phys. Chem. Lett. 2020, 11, 1981−1988